

Myosin Drives Retrograde F-Actin Flow in Neuronal Growth Cones

C. H. Lin,* E. M. Espreafico,[†] M. S. Mooseker,[‡] and P. Forscher[‡]

*National Yang-Ming University
Taipei, Taiwan

[†]Department of Morphology
Faculdade de Medicina de Ribeirão Preto-USP, SP
Brazil

[‡]Department of Biology
Yale University
New Haven, Connecticut 06511

Summary

Actin filaments assembled at the leading edge of neuronal growth cones are centripetally transported via retrograde F-actin flow, a process fundamental to growth cone guidance and other forms of directed cell motility. Here we investigated the role of myosins in retrograde flow, using two distinct modes of myosin inhibition: microinjection of NEM inactivated myosin S1 fragments, or treatment with 2,3-butanedione-2-monoxime, an inhibitor of myosin ATPase. Both treatments resulted in dose-dependent attenuation of retrograde F-actin flow and growth of filopodia. Growth was cytochalasin sensitive and directly proportional to the degree of myosin inhibition, suggesting that retrograde flow results from superimposition of two independent processes: actin assembly and myosin-based filament retraction. These results provide the first direct evidence for myosin involvement in neuronal growth cone function.

Introduction

Neuronal growth cones guide axons in the developing nervous system toward distant target sites. Recent evidence suggests that growth cones decode both diffusible and substrate-bound molecular signals during the guidance process (Kennedy and Tessier-Lavigne, 1995; Tessier-Lavigne, 1992) that involves pathfinding, branching, and ultimately, target recognition. All of these behaviors depend on precise regulation of growth cone motility. Bray pioneered investigation of growth cone motility and was the first to observe that inert particles placed on the growth cone surface moved in a retrograde direction, suggestive of an underlying centripetal membrane or actin filament flux (Bray, 1970). Early studies also demonstrated that growth cone motility depended on actin filament assembly (Yamada and Wessells, 1973), and a critical role for actin assembly in axonal guidance emerged when it was shown that axons in the developing grasshopper nervous system lost all pathfinding capabilities when treated with cytochalasin (Bentley et al., 1986). Later, studies characterizing actin dynamics in *Aplysia* growth cones in vitro suggested that the retrograde flux mentioned above was actually due to actin filament assembly at nucleation sites along

the leading edge, followed by retrograde translocation and recycling at a proximal site by filament severing and/or disassembly. This process was referred to as “retrograde flow” (Forscher and Lin, 1991, *J. Cell Biol.*, abstract; Forscher and Smith, 1988; Mitchison and Kirschner, 1988; Smith, 1988; see also Figure 6B).

The peripheral actin ultrastructure of the growth cone has also been well characterized, being composed of two distinct structural domains: filopodia containing arrays of uniformly polarized (barbed end distal) actin filaments, and intervening lamellipodium domains with less polarized filament structure (cf. Figure 6A; Lewis and Bridgman, 1992). Both domains appear to exhibit uniform retrograde flow relative to an external substrate reference, as judged by actin fluorescence photobleaching studies (Lin and Forscher, 1995). Assembly of actin filaments, followed by centripetal displacement relative to the leading cell margin, has been observed in a wide variety of motile cells, and appears to be a fundamental property of directed growth processes and cell migration (Cramer et al., 1994; Bray and White, 1988; Wang, 1985; Fisher et al., 1988; Abercrombie et al., 1970).

In our initial characterization of actin filament dynamics in *Aplysia* growth cones, we noted that when cones were treated with cytochalasin, retrograde flow did not appear to be markedly affected. Continued retrograde flow in the absence of new actin assembly resulted in formation of an F-actin-free gap along the growth cone margin, and eventual clearance (typically in ~3 min) of F-actin from lamellipodia and filopodia. This persistent retraction of actin filament networks in the absence of actin assembly demonstrated that polymerization could not be supplying the driving force for retrograde F-actin flow; therefore, we suggested that a myosin-like molecular motor might be involved (Forscher and Smith, 1988). Despite recent molecular cloning of several brain myosins (Bahler et al., 1994; Ruppert et al., 1993; Cheney et al., 1993) and localization of myosins to growth cones (Rochlin, 1995; Espreafico et al., 1992; Cheng et al., 1992; Miller et al., 1992), little or no information regarding the functional role of myosins in growth cone motility has emerged to date (cf. Tanaka, 1995).

Given the functional implications of our previous work, we designed experiments aimed at global inhibition of myosin activity, to test whether any myosin was in fact involved in driving retrograde F-actin flow in growth cones. All known myosins have an evolutionarily conserved N terminal head domain containing the ATP, F-actin-binding, and force generation sites (Mooseker and Cheney, 1995). Chymotryptic digestion of muscle myosin results in cleavage of a head domain subfragment (S1) from the rest of the molecule (Margossian and Lowey, 1982). S1 exhibits ATP-dependent actin filament binding, but lacking the C terminal tail, is incapable of generating force unless artificially tethered (e.g., by an antibody) to a substrate. In addition, further treatment of S1 with the sulfhydryl reagent, N-ethylmaleimide (NEM), results in a myosin head species (NEM-S1) that remains tightly bound to actin filaments, even in the presence of ATP, and thus can serve as a potent specific inhibitor

Table 1. ATP-Dependent F-Actin Interactions with S1 and NEM-S1

	S1		NEM-S1	
	-	+	-	+
ATP (2 mM)	-	+	-	+
Percent Protein cosedimented with actin filaments	95 ± 1	7 ± 1	81 ± 8	75 ± 3

of actomyosin function (Cande, 1986; Meeusen and Cande, 1979). Our first experimental approach was then to competitively inhibit myosin function by injection of purified S1 or NEM-S1, and look at effects on growth cone motility, actin dynamics, and structure.

We then compared these results with those obtained after treatment, with 2,3-butanedione-2-monoxime (BDM), a pharmacological inhibitor of endogenous myosin ATPase activity. BDM has previously been shown to effect cross-bridge kinetics and inhibit both conventional muscle and nonmuscle myosin ATPases, including myosin V, platelet myosin II, and a drosophila myosin ATPase fraction, without affecting kinesin ATPase activity or actin assembly (Backx et al., 1994; Cramer and Mitchison, 1995; McKillop et al., 1994; Schramm et al., 1994; Zhao and Kawai, 1994). We show here that both types of myosin inhibition result in essentially the same effects: attenuation of retrograde F-actin flow accompanied by filopodial, and leading edge extension at rates directly proportional to the degree of flow inhibition. These experiments suggest that simple superimposition of two additive processes: actin polymerization, and the action of myosin motors underlie retrograde F-actin flow.

Results

Structural and Functional Changes Induced by S1 or NEM-S1 Microinjection

Table 1 summarizes the results of F-actin cosedimentation assays performed on S1 and NEM-S1 preparations. S1 bound to F-actin in the absence but not in the presence of ATP. The ATP-dependent release of S1 from F-actin was nearly abolished by NEM-modification. These results are consistent with previous reports on NEM-modified heavy meromyosin (Meeusen and Cande, 1979). In control experiments where S1 or NEM-S1 proteins were centrifuged in the absence of actin filaments ± ATP, no protein was detected in the pellet fraction (data not shown).

The S1 proteins prepared for microinjection were further characterized by Western blot analysis (Figure 1A) and immunofluorescence on cultured neurons (Figure 1B). When resolved by SDS-PAGE and stained with Coomassie Brilliant blue, purified S1 or NEM-S1 subfragment preparations contained one major ~100 kDa protein (Figure 1A, lanes 1 and 3). A monoclonal antibody, F59, against the head domain of vertebrate skeletal muscle myosin-II, recognized this major protein and two other minor lower molecular weight species (lanes 2 and 4, Figure 1A); the latter are likely due to limited proteolysis of the S1 and NEM-S1 proteins; their concentrations were less than one tenth that of the ~100 kDa protein species. In addition, Western blot analysis of *Aplysia* CNS (lanes 5 and 6, Figure 1A) and immunofluorescence of uninjected cultured *Aplysia* neurons (data not shown) with the F59 antibody resulted in essentially no immunoreactivity, indicating that endogenous *Aplysia* myosins were not recognized by F59.

Myosin antagonists were typically microinjected into the cell body (arrow, Figure 1B), along with rhodamine-dextran (10–40 kDa) as a volume indicator. Microinjection of S1 or NEM-S1 proteins resulted in characteristic structural and functional effects on the peripheral growth cone lamella (Figure 1). These effects were associated with the presence of exogenous myosin proteins in the cell body and the growth cone region (dashed box, Figure 1B) of the injected cell, as evidenced by positive labeling with the F59 antibody. Growth cones used for injection studies were typically <50 μm away from the cell body, to facilitate rapid diffusion into the growth cone region. Control injections of buffer alone or rhodamine-dextran resulted in no obvious effects on growth cone motility or structure (data not shown). A typical example of the effects of S1 microinjection is shown in Figures 1C–1E. Progressive elongation of filopodia was observed (white arrowheads; Figures 1C–1D) 3 min after injection of S1 protein. Rhodamine-phalloidin staining revealed a high concentration of actin filaments in these newly extended filopodia (Figure 1E).

NEM-S1 injection resulted in similar effects; however, NEM-S1 was more potent and its effects reversed more slowly than S1, as expected from the cosedimentation results. Under control conditions or immediately after microinjection, the ruffling transition zone was typically situated between the peripheral lamellipodium and the central microtubule-rich cytoplasmic domain (Forscher and Smith, 1988). Within ~30 s of NEM-S1 microinjection injection, filopodia extended over time (Figure 1F, open

Figure 1. Effects of S1 and NEM-S1 Microinjection on *Aplysia* Growth Cones

(A) Western blot analysis using F59 monoclonal antibody. Purified S1 (lanes 1 and 2), NEM-S1 (lanes 3 and 4), and protein preparation from whole *Aplysia* nervous tissue (lanes 5 and 6) were either stained with Coomassie Brilliant blue (lanes 1, 3, and 5) or probed with F59 antibody (lanes 2, 4, and 6).

(B) S1 (or NEM-S1) protein was microinjected at the cell body (arrow). Injected protein revealed by F59 immunofluorescence; growth cone region: dashed box.

(C and D) S1 subfragments at concentration of 7.9 mg/ml were injected into the cell shown at lower magnification in (B). DIC images of the growth cones taken before (C) and 3 min after microinjection (D). Note filopodia elongation (arrowheads).

(E) Extended filopodia (arrowheads) contain actin filaments, as revealed by rhodamine-phalloidin staining (identical fields: [D], [E]).

(F) Analysis of growth dynamics following NEM-S1 (2.9 mg/ml) microinjection. Note the initial progressive elongation of filopodia (open arrowheads) and subsequent retraction (closed arrowhead). Expansion of ruffling domain (asterisks) was also apparent. Time (in s) after microinjection is indicated. Bar represents 5 μm.

(G) Retrograde F-actin flow is attenuated after NEM-S1 microinjection. Retrograde flow rates before and after microinjection of either rhodamine-dextran control vehicle) or 4.2 mg/ml NEM-S1 were measured using flow-coupled bead markers. Time = 0 min indicates NEM-S1 microinjection.

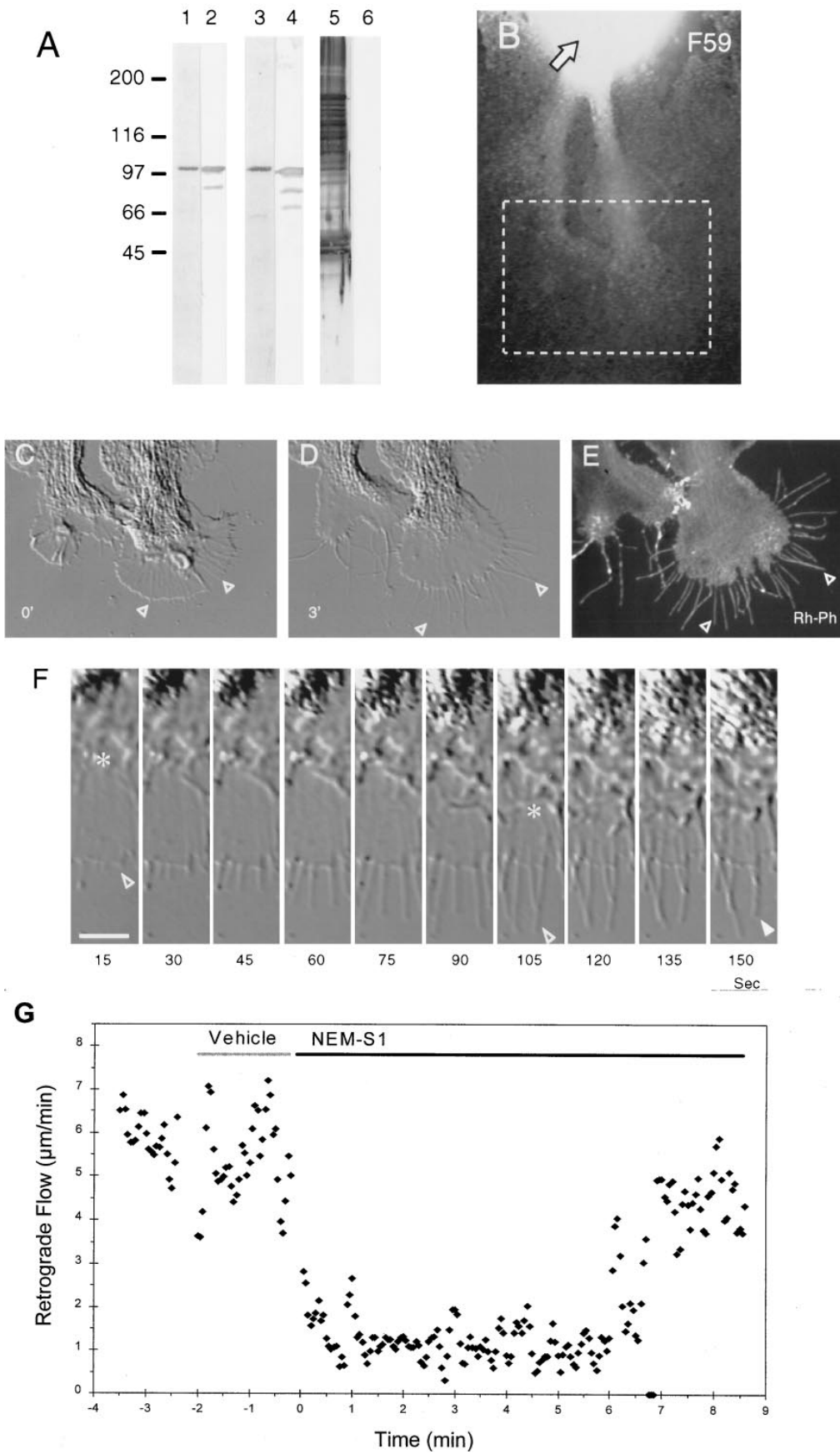


Table 2. Dose Dependence of Retrograde F-Actin Flow Attenuation by NEM-S1

NEM-S1* (μM)	Control	NEM-S1	% Control Rate	Average
	Retrograde	Flow ($\mu\text{m}/\text{min}$)		
1.2	113.00	85.80	75.93	80.44 \pm 6
	113.00	96.00	84.96	
1.9	113.00	94.70	83.81	87.31 \pm 6
	90.00	84.30	93.67	
	90.00	76.00	84.44	
2.3	80.00	56.50	70.63	65.09 \pm 8
	85.30	50.80	59.55	
2.8	113.00	88.00	77.88	66.34 \pm 19
	90.00	68.00	75.56	
	76.00	35.00	46.05	
3.4	85.30	56.20	65.89	43.15 \pm 14
	83.50	24.00	28.74	
	80.00	34.60	43.25	
4.9	85.30	49.00	57.44	35.65 \pm 8
	83.50	24.80	29.70	
	113.00	47.00	41.59	

* assuming $\sim 1/10$ cell volume injections.

Flow rates = mean \pm SD

arrowheads), and the ruffling transition zone often appeared to expand outward (Figure 1F, white asterisks). Initial rates of extension appeared similar for all filopodia within a given growth cone. In this example, the filopodium indicated (white arrowheads) elongated during the first 105 s after injection, then shortened somewhat between 105–150 s (closed arrowhead). The duration of elongation varied, ranging from 1–10 min ($N = 17$ experiments), resulting in filopodia of different lengths. These effects tended to reverse spontaneously over time; however, filopodia shortening appeared to be much slower, occurring in a less synchronous manner than initial filopodium elongation. Growth cones of NEM-S1 injected cells often exhibited leading edge extension; however, the degree of extension tended to vary along the extent of the leading edge, with more pronounced advance typically occurring toward the front of the growth cone. In NEM-S1 experiments where extension of filopodia and leading edge occurred simultaneously, the extent of outgrowth was always more robust in filopodia than the leading edge (data not shown). Actin filament network geometry may be playing a role here; since filopodia contain unidirectional actin filaments oriented parallel with the direction of growth whereas lamellipodia are characterized by a less-polarized filament organization, filopodial protrusion driven by actin assembly may be more efficient.

The structural effects of NEM-S1 microinjection were accompanied by attenuation of retrograde F-actin flow. To measure F-actin flow rates, we utilized membrane-bound flow-coupled beads previously demonstrated to be reliable noninvasive markers for quantitating actin network dynamics in this system (Lin and Forscher, 1995). Beads were rapidly positioned in the desired area of interest using a laser trap, and average bead translocation rates were measured before and after NEM-S1 injection. A typical example is shown in Figure 1G. Control flow rates before microinjection were 5.90 ± 0.79 $\mu\text{m}/\text{min}$ (mean \pm SEM), and no significant change (5.37 ± 1.18 $\mu\text{m}/\text{min}$) was observed in cells microinjected with rhodamine-dextran alone (vehicle). However,

injection of NEM-S1 resulted in rapid dose-dependent attenuation of retrograde flow (NEM-S1; Figure 5D); the retrograde flow rate decreased to 1.16 ± 0.61 $\mu\text{m}/\text{min}$ between 1–6 min after injection, and spontaneously recovered to 4.47 ± 1.01 $\mu\text{m}/\text{min}$ after ~ 7 min. Table 2 and Figure 5D show dose-response data for NEM-S1 injection experiments. Cellular NEM-S1 concentrations were estimated assuming $\sim 1/10$ cell volume injections.

Pharmacological Inhibition of Myosin Activity Mimics S1 Microinjection

To further investigate the effects of myosin inhibition on growth cones, we treated cells with BDM, a myosin ATPase inhibitor. BDM treatment resulted in similar effects to those observed after S1 or NEM-S1 microinjection: attenuation of retrograde flow accompanied by rapid growth. Figure 2A demonstrates typical effects of BDM treatment, including progressive filopodium elongation (arrowheads), leading edge extension (arrows), and a slight retraction of the central cytoplasmic domain. Note the net widening of the lamellipodium during BDM treatment. In the continuous presence of BDM, leading edge and filopodial advance typically continued for 5–10 min, then gradually stopped, despite persistent attenuation of retrograde flow.

BDM treatment also resulted in dose-dependent attenuation of retrograde F-actin flow (Figure 2B). Maximal depth of flow attenuation occurred about 4 min after drug application (Figure 2B, shaded bars), and persisted as long as the drug was present. Retrograde flow recovered to control levels 5–6 min after BDM washout. Table 3 and Figure 5D show dose-response data pooled by normalizing flow rates measured 4 min after drug addition by the control flow rates. Overall, BDM effects on both structure and motility were strikingly similar to those observed after either S1 or NEM-S1 injections (cf. Figure 1).

Structural effects of BDM on the growth cone cytoskeleton were further examined by visualization of

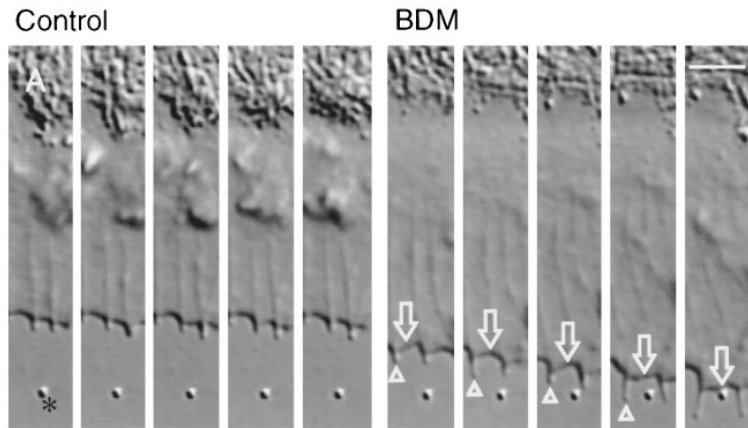


Figure 2. Pharmacological Myosin Inhibition Mimics Effects of NEM-S1 Microinjection

(A) DIC image sequence of a growth cone before (Control) and during treatment with 30 mM BDM. Note the progressive filopodia elongation (arrowheads) and the concomitant leading edge extension (arrows). Asterisk indicates a bead on the substrate for reference. Sampling interval per panel = 15 s. Bar represents 5 μ m.

(B) BDM treatments attenuate retrograde F-actin flow. Note that flow attenuation appears to be dose-dependent, and growth cone exhibits complete recovery after drug washout.

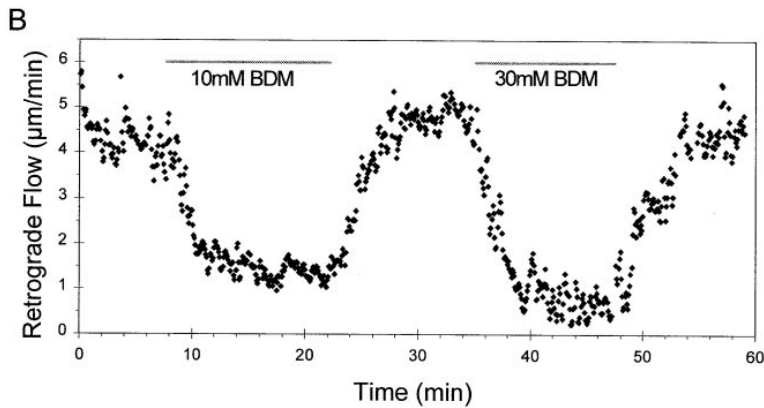


Table 3. Dose Dependence of Retrograde F-Actin Flow Attenuation by BDM

BDM (mM)	Control	BDM	% # Control Rate	Average
	Retrograde	Flow (μ m/min)		
1	6.04 \pm 0.47 (22)#	6.10 \pm 0.56 (26)	101	91 \pm 8
	4.68 \pm 0.35 (21)	4.55 \pm 0.49 (20)	97	
	6.15 \pm 0.41 (16)	5.24 \pm 0.43 (25)	85	
	3.98 \pm 0.38 (16)	3.27 \pm 0.41 (18)	82	
5	3.88 \pm 0.39 (20)	2.94 \pm 0.26 (19)	76	70 \pm 5
	4.95 \pm 0.42 (23)	3.66 \pm 0.39 (21)	74	
	6.15 \pm 0.44 (16)	4.14 \pm 0.42 (27)	67	
	4.36 \pm 0.39 (15)	2.80 \pm 0.34 (19)	64	
10	3.20 \pm 0.27 (9)	2.07 \pm 0.29 (22)	65	56 \pm 8
	4.99 \pm 0.34 (20)	3.19 \pm 0.38 (39)	64	
	4.93 \pm 0.36 (18)	2.93 \pm 0.26 (25)	59	
	3.32 \pm 0.29 (13)	1.84 \pm 0.28 (24)	55	
30	4.37 \pm 0.38 (21)	1.60 \pm 0.25 (23)	37	32 \pm 12
	3.85 \pm 0.33 (16)	1.86 \pm 0.25 (18)	48	
	6.21 \pm 0.45 (14)	2.47 \pm 0.29 (14)	40	
	5.23 \pm 0.40 (19)	1.99 \pm 0.26 (20)	38	
50	5.80 \pm 0.46 (26)	1.01 \pm 0.33 (25)	17	15 \pm 4
	4.37 \pm 0.38 (21)	0.76 \pm 0.21 (18)	17	
	5.47 \pm 0.44 (17)	1.08 \pm 0.26 (18)	20	
	3.04 \pm 0.23 (6)	0.55 \pm 0.27 (19)	18	
	5.16 \pm 0.33 (10)	0.93 \pm 0.36 (24)	18	
	4.93 \pm 0.29 (19)	0.49 \pm 0.18 (16)	10	
	4.26 \pm 0.30 (15)	0.37 \pm 0.17 (15)	9	

Flow rates = mean \pm SD

= Number of flow calculations done

F-actin and tubulin arrays by fluorescence microscopy (Figure 3). Over time, filopodia tended to elongate and accumulate F-actin. In contrast, microtubule distribution appeared to be relatively unperturbed even after prolonged BDM treatments. There also appeared to be a gradual proximal to distal depletion of actin filaments in lamellipodia.

BDM or S1/NEM-S1 Induced Extension Depends on Actin Polymerization

Filopodium and leading edge extension observed following myosin inhibition could result either from actin assembly or translocation of preexisting actin filaments. To differentiate between these two mechanisms, we used cytochalasin B (CB) to inhibit barbed end actin polymerization during BDM (Figure 4A), or S1 microinjection (data not shown) induced filopodium elongation. As shown in Figure 4A, filopodium elongation was first triggered by BDM treatment (white line, 0–40 s). Subsequently, exposure to 1 μ M CB in the presence of BDM immediately eliminated further filopodium extension (dashed line, 50–90 s). Finally, washout of CB in the presence of BDM resulted in resumption of filopodial extension at nearly pre-CB rates (black line, 100–150 s). These results indicate that barbed end actin assembly drives the protrusive growth observed during BDM treatments and S1/NEM-S1 microinjections.

Actin Network Translocation during Cytochalasin Treatment Is Myosin-Dependent

Our previous work demonstrated a characteristic pattern of persistent retrograde actin network retraction during cytochalasin treatment (described above and in Forscher and Smith, 1988; Lin and Forscher, 1993), suggesting that the translocation aspect of retrograde flow did not depend on actin assembly. To examine the role of myosin in this response, we observed the effects of BDM treatment on F-actin network movement in the absence of actin assembly. Since the onset of BDM effects are slower than CB (\sim 3.0 versus \sim 0.25 min respectively), growth cones were pretreated with BDM to attenuate retrograde flow before addition of CB (Figure 4B, note nonlinear time points shown in individual panels, asterisks). After 1 min in 30 mM BDM, filopodium elongation was apparent (Figure 4B, 2 min, arrowhead) and substantial slowing of retrograde flow was observed. At this point, CB was added and combined CB/BDM treatment resulted in slow retraction of F-actin from the leading edge (bars indicate F-actin free gap formation). Note that retraction rates in CB/BDM were very slow in the 2–5 min interval, and then stalled completely during the 5–9 min interval. This 4 min stall period is significant since under control conditions, it typically takes less than 3 min for a filament at the leading margin to transverse the entire lamellipodium. At 9 min, myosin inhibition was relieved by BDM wash out and resulted in retraction of residual actin networks (9–13 min). Note that retraction resumed (in CB) at 4.85 μ m/min, which is similar to retrograde flow rates observed under control conditions (Forscher and Smith, 1988). The growth cone fully recovered after CB washout (20 min recovery).

Filopodium Extension and Retrograde F-Actin Flow Rates Are Inversely Proportional

Since myosin inhibition resulted in simultaneous attenuation of retrograde F-actin flow and filopodium extension, we investigated how these two phenomena were related. To quantitate F-actin movement, flow coupled bead markers were positioned with a laser trap at the same location on the lamellipodium before and after myosin inhibition treatments, as in Figures 5A–5C. Note in this example that under control conditions, retrograde flow (Figure 5B, black vector, rate = 5.10 mm/min) is accompanied by essentially no filopodium extension (white dashed line). Two min after application of 10 mM BDM, retrograde flow decreased to about 54% of the control rate (Figure 5C, black vector, rate = 2.75 mm/min) and filopodium extension occurred (white dashed line, rate = 2.21 mm/min). Similar data analyses were performed on growth cones treated with different concentrations of BDM (Figure 5E, open circles, 29 experiments) or microinjected with 2–4 mg/ml NEM-S1 that translates into intracellular protein concentrations of 2–4 mM assuming a \sim 1/10 cell volume injections (Figure 5E, closed squares, 17 experiments). Retrograde flow rates decreased with either increasing BDM dose or amount of NEM-S1 protein injected (Figure 5D). When the dose-response data from both types of inhibitor studies were pooled and filopodium growth plotted against retrograde F-actin flow rates, an inverse linear relationship was apparent, strongly suggesting that filopodia growth and retrograde flow are simple additive processes with opposite sign (Figure 5E).

Discussion

Myosin(s) Drives Retrograde F-Actin Flow in Neuronal Growth Cones

In this study, we present two independent lines of evidence that retrograde F-actin flow in growth cones is driven by a myosin-type molecular motor: competitive inhibition by injection of purified S1 or NEM inactivated myosin head domain subfragments (NEM-S1), and pharmacological inhibition of myosin ATPase activity with BDM. Both treatment regimes resulted in strikingly similar effects on growth cone motility and structure, specifically, dose-dependent attenuation of retrograde F-actin flow accompanied by marked filopodial, and in the case of BDM, leading edge growth. The significance of each of these effects will be examined below.

Both S1 and NEM-S1 compete with endogenous myosin(s) for actin filament binding sites, and can thus be used as tools for studying actomyosin function. Because NEM-S1 binds actin filaments essentially irreversibly, it should be a more potent competitive antagonist as was observed here. In contrast with the S1 or NEM-S1 protein reagents that directly interact with actin filaments, evidence suggests that BDM is a general myosin ATPase inhibitor (Cramer and Mitchison, 1995; Higuchi and Takemori, 1989; Schramm et al., 1994; Steinen et al., 1995). BDM is thought to act by stabilizing the weak actin-binding myosin-ADP-P_i intermediate state (Herrmann et al., 1992) and has seen wide use in muscle physiology (Alpert et al., 1989; Fryer et al., 1988; Gwathmey et al., 1992; Horiuti et al., 1988; Steele and Smith, 1993; Tung

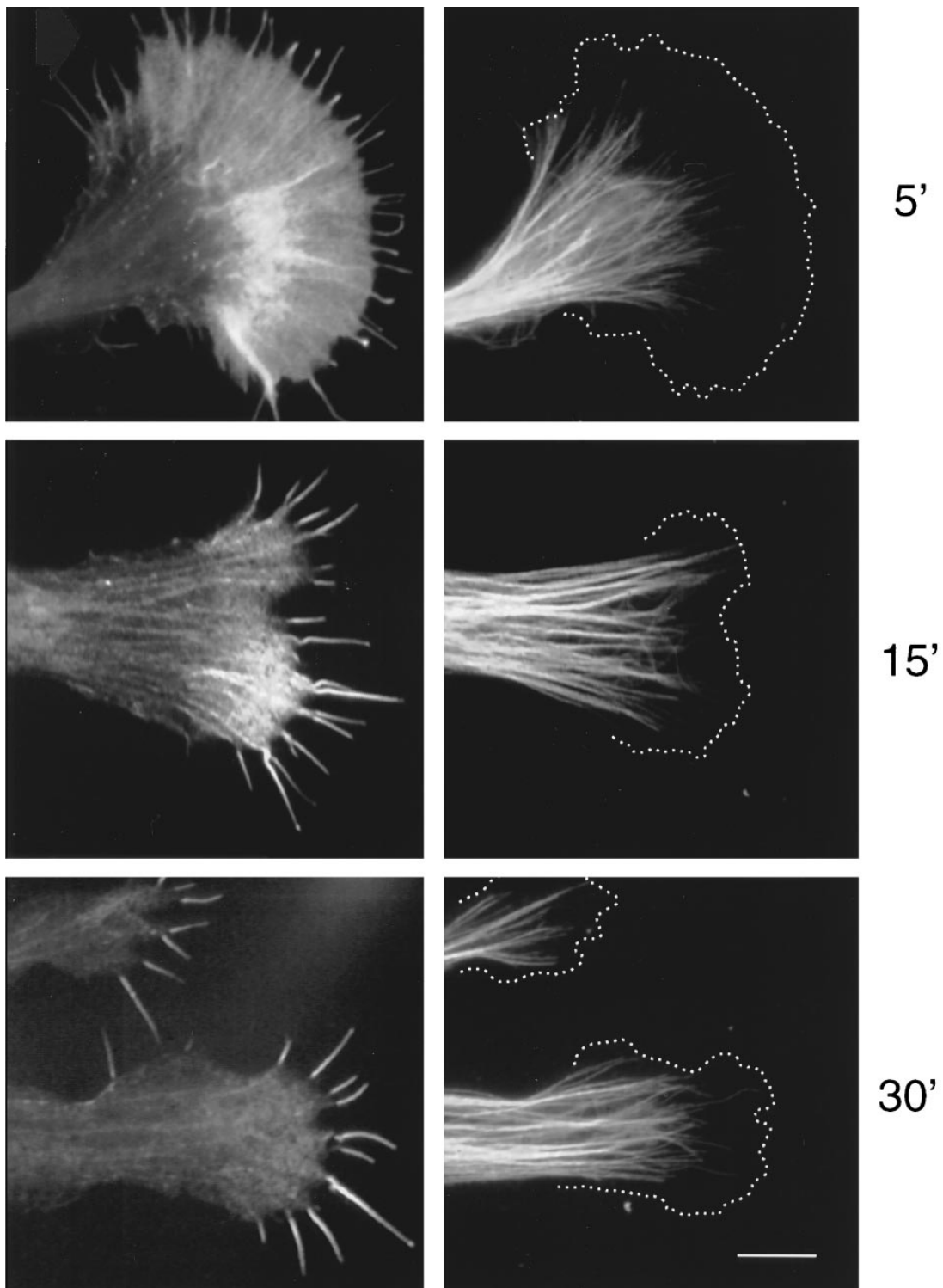


Figure 3. Changes in Cytoskeletal Structure after BDM

Cells were treated with 10 mM BDM for: 5, 15, and 30 min. F-actin structures (left) of the growth cone were revealed by rhodamine-phalloidin staining and microtubule distribution (right) by β -tubulin immunofluorescence. Dotted lines in β -tubulin panels indicate leading edges of the individual growth cones. Bar represents 10 μ m.

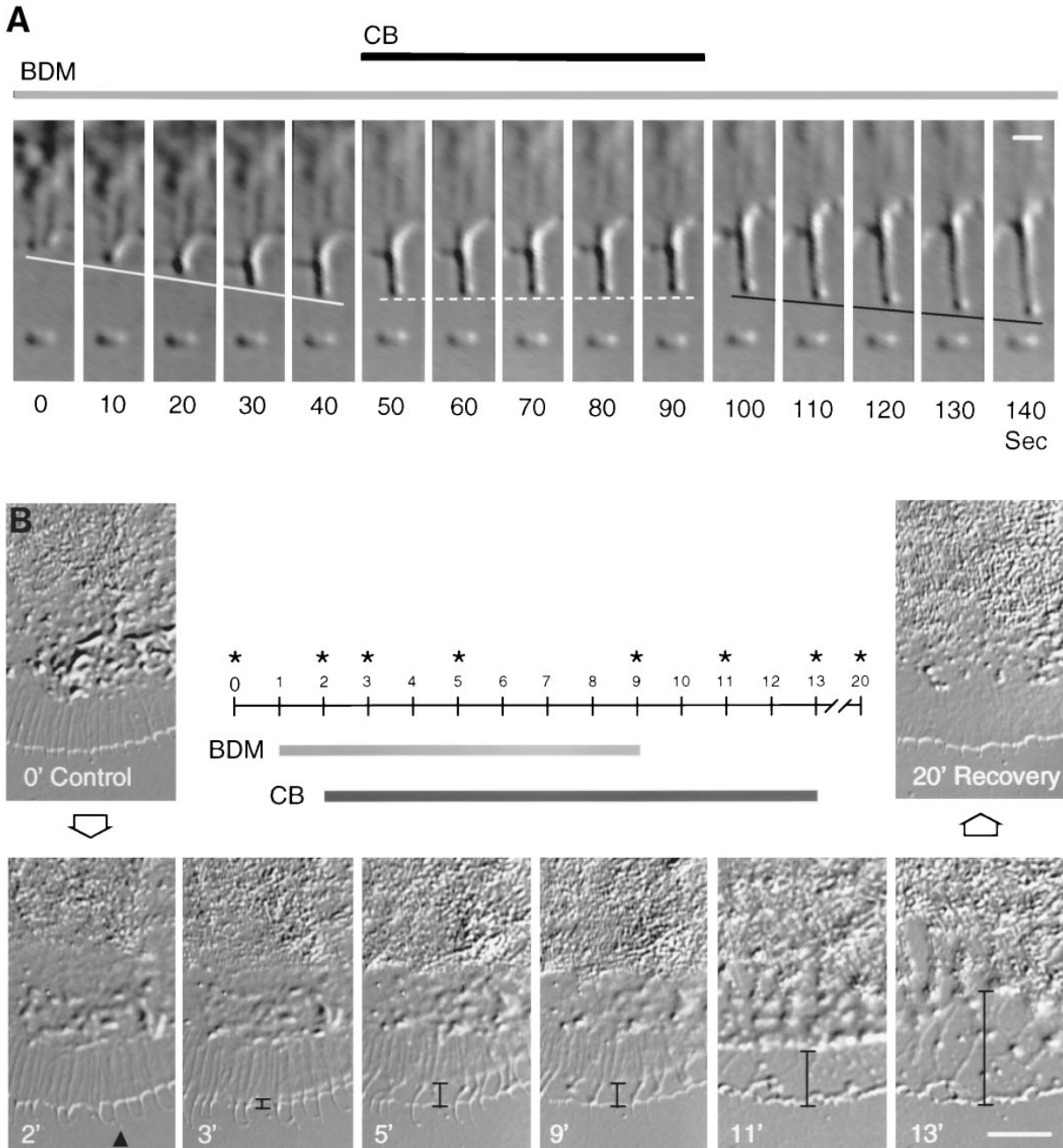


Figure 4. Actin Assembly and Myosin Motors Drive Independent Processes

(A) Actin assembly drives filopodium protrusion. Initial application of 10 mM BDM triggers filopodium elongation (0–40 s) at 5.6 $\mu\text{m}/\text{min}$. Elongation was reversibly inhibited by adding 1 μM cytochalasin B (CB) to the BDM solution (50–90 s). Washout of the CB in the continuous presence of BDM results in resumed outgrowth of the stalled filopodium at 4.62 $\mu\text{m}/\text{min}$ (100–140 s). Time intervals for the sequence = 10 s. Bar represents 2 μm .

(B) Myosin drives actin network retraction in the presence of CB. Pretreatment with 30 mM BDM resulted in filopodium elongation (black arrowhead). After 1 min in BDM, 5 μM CB was added. Combined CB/BDM treatment induced gap formation as a result of breakaway of F-actin from the leading edge (black line, 3 min CB/BDM). Retraction of residual actin networks was initially very slow, and later stopped completely (5–9 min CB/BDM interval). Washout of BDM in the presence of CB resulted in retraction of residual actin networks (black line, 11–13 min CB). Full recovery was observed after CB washout (20 min recovery). Images shown are indicated by asterisks in experimental protocol timeline. Bar represents 10 μm .

et al., 1985; West and Stephenson, 1989), where, not surprisingly, it acts as a relaxant.

A major concern with pharmacological agents such as BDM is specificity of action: are there contaminating

side effects? A parallel concern with competitive inhibitors is that although their site of action may be specific, secondary effects may be incurred by displacement of proteins other than the targeted effector molecule; for

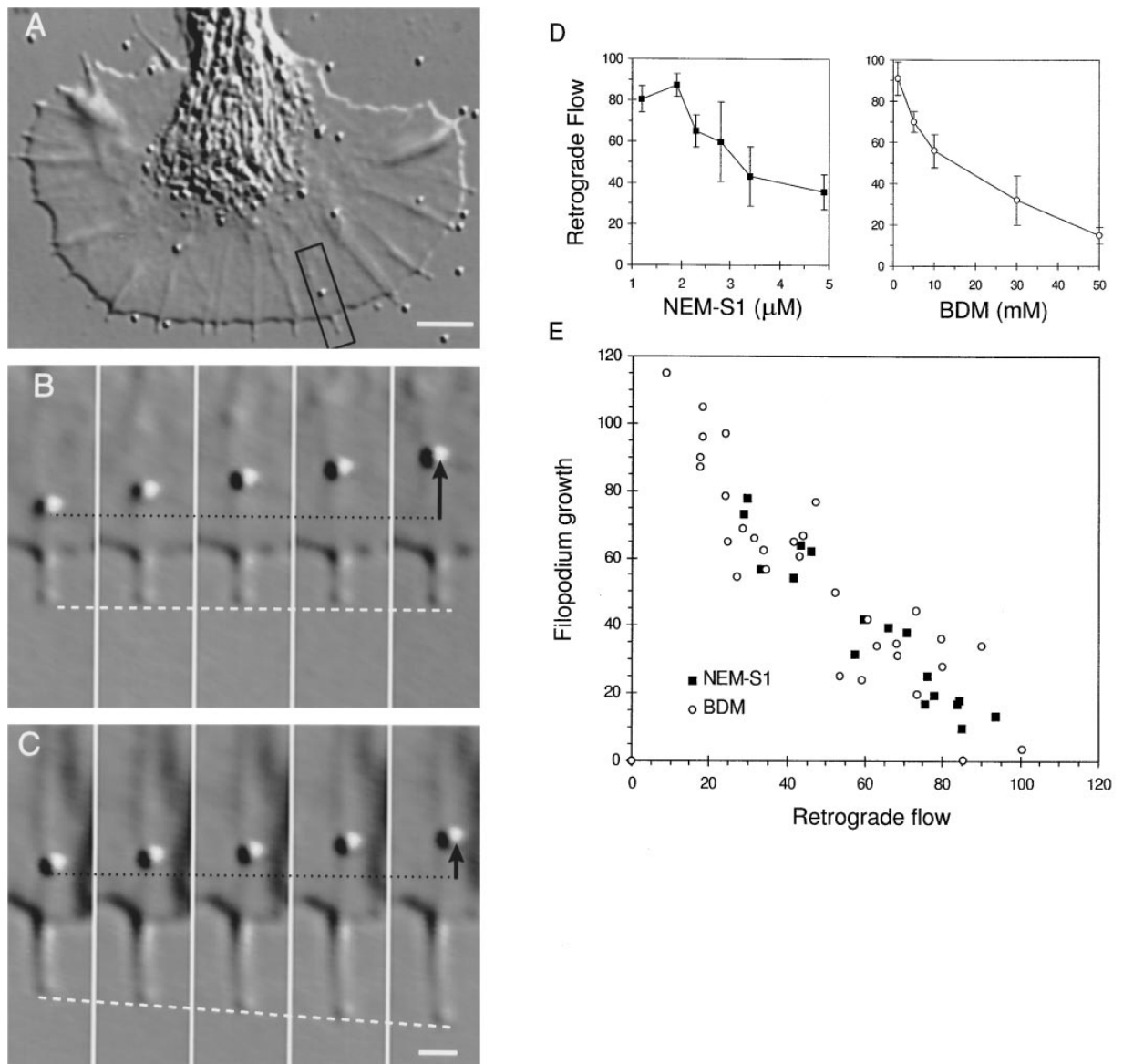


Figure 5. Rates of Filopodium Growth and Retrograde F-Actin Flow Are inversely Proportional

- (A) To compare the rates of F-actin flow before and after treatments that inhibited myosin activity, 200 nm beads were positioned at the same location (box) using the laser trap. Bar represents 5 μm .
 (B) Robust retrograde F-actin flow (black dashed line) and little, if any, filopodium outgrowth (white dashed line) were observed under control conditions.
 (C) After application of 10 mM BDM, filopodium elongation (white dashed line) occurred along with slowing of retrograde F-actin flow (black dashed line). Bar represents 1 μm .
 (D) Dose-response curves for NEM-S1 and BDM treatments. Rates are % control retrograde flow. See Tables 2 and 3 for details.
 (E) Rates of filopodium elongation versus retrograde flow. Data from different experiments (growth cones) were normalized by control retrograde flow rates.

example, NEM-S1 might displace actin binding proteins involved in regulation of actin dynamics and/or network structure. In this study, we found that both types of myosin inhibition scheme (S1/NEM-S1 or BDM treatment) led to nearly identical structural changes and effects on growth cone motility. This occurred despite the disparate mechanisms of action embodied by the two treatments. It is highly unlikely that we would observe such similar effects from such dissimilar agents unless

both were working through a common effector, i.e., myosin(s).

High concentrations (>50 mM) or long term (>30 min) BDM treatments were accompanied by progressive decreases of F-actin content in lamellipodia (Figure 3). In addition, although retrograde flow was inhibited as long as the BDM was present (Figure 2B), filopodia extension occurred predominantly in the first 15 min after drug application. These observations raise the issue of BDM

side effects on actin metabolism. Cramer and Mitchison (1995) have recently shown that overnight treatment with 20 mM BDM had no effect on *in vitro* actin assembly, and we show here that filopodial protrusion induced by 10 mM BDM was due to continued barbed end assembly (Figure 4A). These observations make it unlikely that the decreased flow rates we observed shortly after BDM treatment resulted from actin related side effects. We also noted that the ED_{50} for BDM mediated retrograde flow attenuation was slightly higher than that recently reported for inhibition of postmitotic spreading in PtK2 cells (Cramer and Mitchison, 1995). This difference likely reflects lower BDM solubility in the high salt marine saline (ASW) used here than in the lower ionic strength PBS used in the PtK2 study.

Finally, the pattern of F-actin signal decay over time after BDM treatment that can be seen in Figure 3 is worth a short comment. Under control conditions retrograde flow delivers actin filaments to the proximal transition zone at a rate of ~ 100 nm/s (Mitchison and Kirschner, 1988; Smith, 1988). To maintain steady state, the growth cone must take apart or "recycle" these networks approximately as fast as they arrive (cf. Figure 6B). It is likely that this filament recycling involves severing and a yet uncharacterized accelerated disassembly process, since it is too fast to be accounted for by simple actin disassembly rates measured *in vitro* (Pollard, 1986; Pollard and Cooper, 1986). In any case, the anterograde spreading decay of lamellar F-actin over time we observe might result from continued action of the filament recycling process in the absence of retrograde flow.

Actin Assembly Drives Protrusion and Myosin Drives Retrograde Flow Independently

Both S1/NEM-S1 and BDM treatments resulted in moderate leading edge extension and marked filopodial growth (Figures 1–3) that was totally and reversibly inhibited by low doses of cytochalasin (Figure 4), demonstrating that protrusive growth can be accounted for by barbed end actin filament assembly without invoking alternative mechanisms, such as actin filament sliding. In addition, we found that retrograde movement of (residual) actin networks in CB was reversibly inhibited by BDM (Figure 4B), indicating that in the absence of actin assembly, retrograde movement of F-actin depends critically on myosin motor action, as originally proposed (Forscher and Smith, 1988). These complimentary experiments demonstrate that protrusive growth and retrograde flow are experimentally separable processes, and suggest that the respective underlying mechanisms of actin assembly and myosin powered network retraction are independent. If the latter suggestion were true, growth and retrograde flow would be expected to be additive processes of opposite sign; i.e., they would be inversely proportional. Indeed, when filopodial growth was plotted versus retrograde flow under varying degrees of myosin inhibition, an inverse linear relationship was readily apparent (Figure 5). It should also be noted here that previous studies have shown that S1 can promote actin assembly *in vitro* (Grazi et al., 1980; Detmers et al., 1981). S1 exhibits 1:1 stoichiometric binding to

actin filaments and the acto-S1 complexes appear to function as hyperstable actin nucleation sites (Miller et al., 1988). This property of S1 does not really affect our interpretation of the effects of S1/NEM-S1 on retrograde flow; however, it does raise the possibility that the filopodial growth we observe might be simply due to potentiation of actin assembly by S1 or NEM-S1. As mentioned above, BDM has little or no effect on *in vitro* actin assembly (Cramer and Mitchison, 1995), yet BDM treatment consistently led to robust leading edge and filopodial extension (e.g., Figure 2A). Although we can not rule out permissive effects of S1 or NEM-S1 on actin assembly, the simple inverse proportionality of the growth versus flow plot for both BDM and NEM-S1 (Figure 5E) suggests that the major initial effect of both treatments is simply slowing of retrograde flow that leads to proportional filopodial growth. Finally, why BDM would elicit leading edge growth more reliably than S1/NEM-S1 injections is not clear. One possibility is that lamellipodia are more easily disrupted than filopodia by agents (like S1 or NEM-S1) capable of interfering with actin cross linking proteins.

Do myosin motors or actin assembly limit the rate of retrograde flow? A flow-coupled bead will move steadily rearward over time, and is not affected by nearby leading edge and filopodia protrusions and retractions (P. F. and C. H. L., unpublished data). This supports the contention that protrusion (assembly) and retrograde flow are uncoupled processes, and also that actin assembly rates can transiently exceed those of retrograde flow. That actin assembly can drive motility at rates in excess of retrograde flow was independently demonstrated during previous characterization of a focal actin assembly response, triggered by highly charged polycationic beads applied to the growth cone surface (Forscher et al., 1992). In this case, actin assembly led to generation of F-actin tails similar to those formed by invasive bacteria such as *Listeria monocytogenes* (Theriot et al., 1992b). We showed that actin assembly could drive bead translocation at up to four times the average retrograde flow rate. Thus, it seems fairly clear that actin assembly rates do not limit retrograde flow, and further studies on myosin regulatory mechanisms in growth cones appear to be in order.

Significance of the Inverse Growth Versus Retrograde Flow Relationship

Aplysia growth cones exhibit a spatially uniform pattern of retrograde F-actin flow and advance very slowly when they are not interacting with target substrates (Lin and Forscher, 1995). Although the naming convention may differ, a wide variety of motile cells also exhibit centripetal flux, cortical flow, or retrograde flow of F-actin. Despite its ubiquitous presence and speculations regarding its importance, the mechanism of retrograde flow has been elusive (Bray and White, 1988; Cramer et al., 1994; Heath and Holifield, 1991). The results of the present study help fill this gap in our knowledge, and suggest a surprisingly simple steady state model can account for the salient features of the retrograde flow. Since both filopodial and lamellipodial F-actin (Figure 6A) appear to move in concert (Lin and Forscher, 1995), we treat

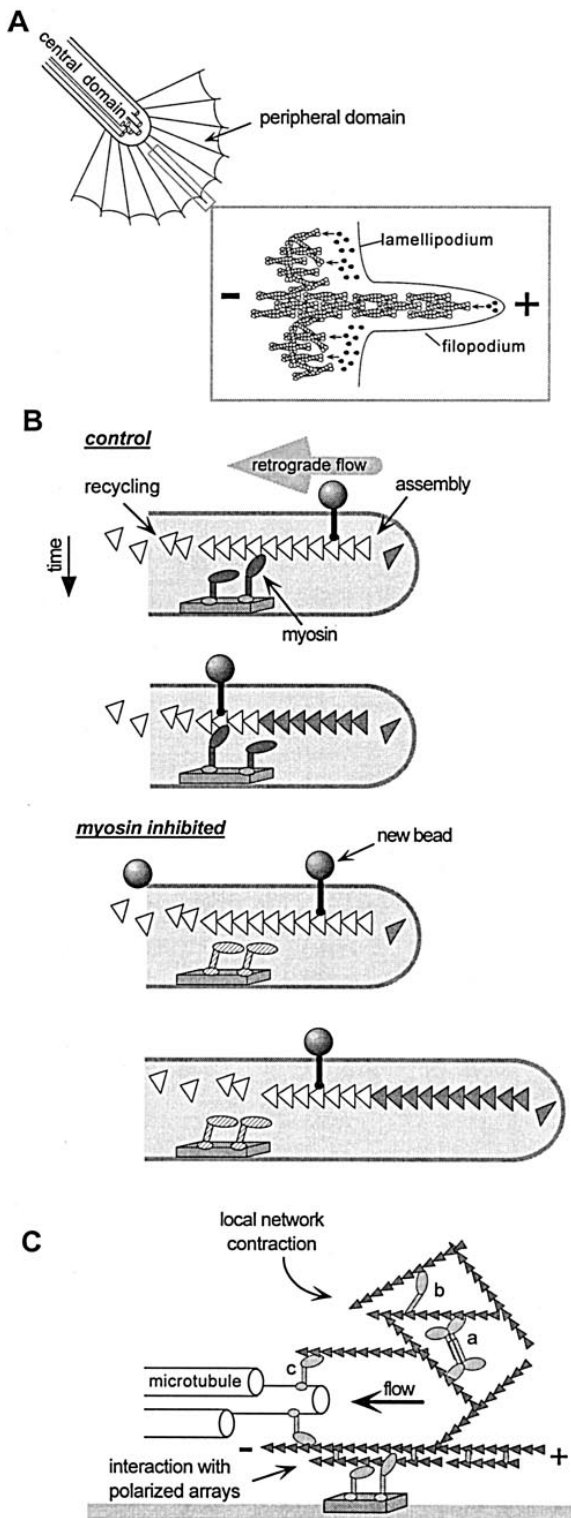


Figure 6. Model
(A) Major structural domains of a growth cone are the microtubule-rich central domain and F-actin-rich peripheral domain comprised of unipolar barbed (+) end distal actin filaments (filopodium) and less polarized intervening cross-linked networks in the lamellipodium. (B) Simplified schematic of myosin inhibition results. Under Control conditions, filopodial length is maintained by actin assembly at the leading margin balanced by retrograde flow driven by myosin mo-

them as a single kinetic unit and make the simplifying assumptions depicted in Figure 6B. Under control conditions, we observe slow growth and robust retrograde flow; actin filaments are moved away from the leading edge by myosin action about as fast as they are assembled (Figure 6B, control). When myosin is inhibited, retrograde flow slows and we observe growth in direct proportion to the degree of flow attenuation (Figure 6B, myosin inhibited). Note that this "growth" involves a net widening of the peripheral domain (cf. Figure 2A), and thus differs markedly from the physiological growth we observe during growth cone target interactions (Lin and Forscher, 1993). In the latter case, synchronous and directed advance of both central microtubule and peripheral lamellar domains is observed, enabling the growth cone to maintain structural equilibrium, despite dramatic increases in its net growth rate.

In contrast with growth cones, which at best advance relatively slowly, cells such as keratocytes can translocate approximately as fast as actin is assembled at their leading margin; therefore, although constant centripetal actin flux in the cell's reference frame occurs, there is little or no retrograde F-actin flow, with respect to an external substrate reference (Theriot and Mitchison, 1991; Theriot and Mitchison, 1992a). It is thought that keratocytes and other highly motile cells employ highly efficient adherence mechanisms to limit actin slippage and thereby keep retrograde flow to a minimum (Lee et al., 1993; Lee et al., 1994). Interestingly, we have recently shown that when growth cones interact with a favorable growth substrate, retrograde flow slows in direct proportion to increased rates of both leading edge and axonal microtubule advance (Lin and Forscher, 1995). We suspect that in this case, flow attenuation results from stabilization of newly assembled actin filaments, with respect to the target substrate by adhesion complexes that may act somewhat like a molecular clutch (Lin et al., 1994; Tanaka, 1995). Note this would not only promote the protrusive growth observed, but in the context of the present study would appear to engage the actomyosin force generation system, perhaps allowing the growth cone to pull the distal axon toward the target substrate.

In the context of directed axonal growth, it is interesting to note that the central domain appeared to recede slightly during myosin inhibition experiments (cf. Figure 2A), and microtubule distribution did not appear to be markedly affected (Figure 3). This kind of response is

tors. Motors are bound to a reference frame stable with respect to an external substrate reference (shaded box). Extracellular flow coupled beads move in synchrony with retrograde F-actin flow (gray arrow). Newly assembled F-actin is shaded. Myosin inhibition attenuates both retrograde flow and bead movement resulting in protrusive growth due to maintained F-actin assembly. Rates of growth and retrograde F-actin flow are inversely proportional.

(C) Generation of centripetal force could be accomplished by the action of conventional (A) or nonconventional (B) myosins either intercalated into less ordered actin networks and acting through a local network contraction mechanism, or alternatively, by interacting with the polarized filopodial actin filament arrays. Possible myosin localization to microtubules in the central cytoplasmic domain could promote microtubule tensioning and directed advance ([C], discussed in text).

very unusual in this system. Nearly all perturbations of growth cone function we have previously encountered including prolonged cytochalasin treatment (cf. Figures 4 and 7; Forscher and Smith, 1988), aging in culture, exposure to phototoxic light levels, osmotic shock, and perturbation of actin structure by various pharmacological agents, result in microtubule extension, rather than recession. An intriguing possibility suggested by these observations is that actomyosin interactions in the growth cone promote microtubule extension either by tensioning microtubules or by a less direct mechanism (cf. Figure 6C). Clearly, this would be advantageous during growth cone target interactions when highly directed microtubule advance is observed (Lin and Forscher, 1993).

These results provide the first functional evidence that myosin motors are involved in generating retrograde flow in growth cones. Given the structural makeup of F-actin in the growth cone, the force generation mechanism might involve localized activation and contraction of myosin molecules intercalated into the less-ordered lamellar actin networks, or myosins interacting with the unipolar actin filament arrays in filopodia (Figure 6C). The functional implications of this study provide a strong impetus for further molecular characterization of the myosin(s) involved, and suggest a conceptual framework for understanding and testing the role of retrograde actin flow in other motile systems.

Experimental Procedures

Preparation of Proteins

Skeletal muscle myosin was purified from chicken pectoralis muscle, according to the method of Kielley and Harrington (1959). Actin was purified from an acetone powder of chicken skeletal muscle, according to the method of Spudich and Watt (1971). S1 proteolytic fragments were prepared from myosin digested with 50 μ g/ml α -chymotrypsin in the presence of 1 mM EDTA-K (Margossian and Lowey, 1982); protease activity was inhibited by addition of 1 mM Pefabloc (Boehringer Mannheim, Indianapolis, IN). NEM-S1 was produced by incubating S1 at 5–10 mg/ml in 50 mM KCl, 20 mM imidazole-Cl (pH 7.2), 1 mM EDTA-K, and 0.1 mM DTT, with 1.0 mM freshly dissolved NEM at room temperature for 20 min. The reaction was stopped by adding DTT to a final concentration of 10 mM; unreacted NEM was removed by dialysis (Meeusen and Cande, 1979). Cytochalasin B (CB) and BDM were purchased from Sigma Chemical Company (St. Louis, MO).

F-Actin Cosedimentation Assay

G-actin at a final concentration of 250 μ g/ml (6 mM) was induced to polymerize by addition of KCl to a final concentration of 75 mM and $MgCl_2$ to 2.5 mM in a 10 mM imidazole, 1 mM EGTA buffer. S1 or NEM-S1 at a final concentration of 150 μ g/ml (1.5 mM) were then added to the F-actin solution either in the absence or in the presence of 2 mM Mg-ATP. As controls, reactions containing only S1 or NEM-S1 without F-actin, or F-actin alone, were also performed. The reactions were incubated at room temperature for 20 min, then centrifuged at 100,000 X g for 45 min at 15°C. Equal amounts of the resulting supernatants and pellets were resolved on a 5%–16% SDS-PAGE and then stained with Coomassie Brilliant blue. The gel was then scanned and digitized using a Scanmaker III (Microtek Laboratory Incorporated, Redondo Beach, CA), and densitometry was performed using Band Leader (Internet ShareWare, Ma'ayan Aharoni). Average values are shown in Table 1 from three experiments using three separate protein preparations.

Cell Culture, Solutions, and Video Microscopy

Cell culture and video microscopy techniques as previously described (Forscher and Smith, 1988; Lin and Forscher, 1993; Lin and

Forscher, 1995). 2,3-butanedione-2-monoxime (Sigma, St. Louis, MO) was dissolved in DMSO before adding to ASW, such that the final concentration of DMSO in working solutions was less than 0.3%. In control experiments, no effects on growth cone structure or motility were observed after 1% DMSO treatment (data not shown).

Microinjection

The microinjection protocol was described previously (Lin and Forscher, 1995). Briefly, bag cell neurons were transferred to a custom-made injection chamber, then the cell bodies were impaled with a glass pipette mounted on a 3D hydraulic micromanipulator (Narashigi USA) retrofitted with a piezoelectric axial drive (Burleigh Instruments, Fishers, NY) under video-enhanced-DIC observation. Purified S1 or NEM-S1 proteins at concentrations of 2–8 mg/ml were loaded in the injection needle together with 0.5 mg/ml 10 kDa rhodamine-dextran (Molecular Probes Incorporated, Eugene, OR) used as a volume indicator. Reagent or vehicle solution injections were typically \sim 10% of cell volume.

Immunoblots and Immunofluorescence

For fluorescent staining of the cytoskeleton, cells were first fixed with 4% freshly made paraformaldehyde in isotonic ASW supplemented with 400 mM sucrose (pH 7.6) (Lin and Forscher, 1993). After fixation, cells were permeabilized for 2–5 min in fixation buffer plus 0.5% Triton-X 0, washed with PBS, and stained with rhodamine-phalloidin (Molecular Probes) in PBS. Cells were then washed with PBS, exposed to 5% bovine serum albumin-PBS, followed by monoclonal mouse anti- β -tubulin antibody (Sigma, St. Louis, MO), washed with PBS, exposed to FITC conjugated goat anti-rabbit secondary antibody (Jackson Labs, West Grove, PA), washed with PBS, transferred to a mounting solution containing PBS supplemented with 20 mM n-propyl-gallate (Sigma) and 80% glycerol/20% PBS, and examined immediately. To localize microinjected S1 or NEM-S1 proteins, F59, a monoclonal antibody made against the head domains of skeletal muscle myosin (provided by Dr. Frank Stockdale, Stanford University) was used. Culture supernatant from the hybridoma cell line was diluted 1:50 for primary antibody incubation. For immunoblot analysis, purified S1 and NEM-S1 proteins or whole protein preparation from *Aplysia* nervous tissue were resolved on a 5%–16% SDS-PAGE gel, transferred to nitrocellulose paper, and then probed with F59 monoclonal antibody at 1:250 dilution and secondary antibody conjugated with alkaline phosphatase.

Surface Markers and Micro-Positioning

To prepare flow-coupled beads for retrograde flow rate measurement, 200–500 nm polystyrene beads (Polyscience, Warrington, PA) or silica beads (Bangs Laboratory Incorporated, Carmel, IN) were either coated with polyethyleneimine (Sigma; Forscher and Smith, 1990; Lin and Forscher, 1995) or derivatized with avidin followed by biotinylated Concanavalin A (Vector Laboratory Incorporated, Burlingame, CA). Beads were then incubated for 10 min in artificial sea water (ASW) supplemented with 1 mg/ml BSA blocking protein before application to cells to inhibit possible triggering of subjacent F-actin assembly by beads (inductopodia formation, see Forscher et al., 1992). An infrared single beam gradient optical trap (Svoboda and Block, 1994) was used to repeatedly position beads at the same location on the growth cone lamella before and after treatments inhibiting myosin activity. The laser trap employed a 150 mW laser diode emitting at 790 nm, as previously described (Lin and Forscher, 1995).

Kinetic Analysis of Retrograde F-Actin Flow

Kinetic analysis was done using programs developed in this laboratory (Forscher et al., 1992; Lin and Forscher, 1993; Lin and Forscher, 1995). To quantitate the changes in retrograde F-actin flow, flow-coupled beads were placed over the entire angular extent of the growth cone lamella before and after S1 or NEM-S1 microinjection or BDM treatment. Translocation rates of individual beads (indicative of underlying F-actin flow rates) were measured during bead transport on the lamella between the leading edge and the proximal transition zone using 5 s sampling intervals. Data was pooled from all beads attached to the growth cone membrane at any given time point; resulting average rates were then plotted as a function of time.

To analyze correlations between the retrograde flow and structural changes (e.g., filopodium elongation), flow-coupled beads were positioned at the same site before and after the treatment using the laser trap. Bead centroid positions were obtained and used to calculate the bead displacement (Lin and Forscher, 1995).

Acknowledgments

This work was supported by National Institutes of Health grants NS28695 to P. F. and R37-DK25387 to M. S. M., a McKnight Endowment Fund for Neuroscience Award to P. F., and a Basic Research Grant from the Muscular Dystrophy Association to M. S. M.

The costs of publication of this article were defrayed in part by the payment of page charges. This article must therefore be hereby marked "advertisement" in accordance with 18 USC Section 1734 solely to indicate this fact.

Received March 5, 1996.

References

- Abercrombie, M., Heaysman, J.E.M., and Pegrum, S.M. (1970). The locomotion of fibroblasts in culture. III. Movement of particles on the dorsal surfaces of leading lamella. *Exp. Cell Res.* **62**, 389–398.
- Alpert, N.R., Blanchard, E.M., and Mulieri, L.A. (1989). Tension-independent heat in rabbit papillary muscle. *J. Physiol.* **414**, 433–453.
- Backx, P.H., Gao, W.D., Azon-Backx, M.D., and Marban, E. (1994). Mechanisms of force inhibition by 2,3-butanedione monoxime in rat cardiac muscle: roles of calcium and crossbridge kinetics. *J. Physiol.* **476**, 487–500.
- Bahler, M., Kroschewski, R., Stoffler, H.E., and Behrmann, T. (1994). Rat myr 4 defines a novel subclass of myosin I: identification, distribution, localization, and mapping of calmodulin-binding sites with differential calcium sensitivity. *J. Cell Biol.* **126**, 375–389.
- Bentley, D., and Toroion-Raymond, A. (1986). Disordered pathfinding by pioneer neuron growth cones deprived of filopodia by cytochalasin treatment. *Nature* **323**, 712–715.
- Bray, D. (1970). The surface movement during growth of single explanted neurons. *Proc. Natl. Acad. Sci. USA* **65**, 905–910.
- Bray, D., and White, J.G. (1988). Cortical flow in animal cells. *Science* **239**, 883–888.
- Cande, W.Z. (1986). Preparation of N-ethylmaleimide-modified heavy meromyosin and its use as a functional probe of actomyosin-based motility. *Meth. Enzymol.* **134**, 473–477.
- Cheney, R.E., O’Shea, M.A., Heuser, J.E., Coelho, M.V., Wolenski, J.S., Espreafico, E.M., Forscher, P., Larson, R.E., and Mooseker, M.S. (1993). Brain myosin-V is a two-headed unconventional myosin with motor activity. *Cell* **75**, 13–23.
- Cheng, T.P., Murakami, N., and Elzinga, M. (1992). Localization of myosin IIB at the leading edge of growth cones from rat dorsal root ganglionic cells. *FEBS Lett.* **311**, 91–94.
- Cramer, L.P. and Mitchison, T.J. (1995). Myosin is involved in postmitotic cell spreading. *J. Cell Biol.* **131**, 179–189.
- Cramer, L.P., Mitchison, T.J., and Theriot, J.A. (1994). Actin-dependent motile forces and cell motility. *Curr. Opin. Cell Biol.* **6**, 82–86.
- Detmers, P., Weber, A., Elzinga, M., Stephens, R.E. (1981). 7-Chloro-4-nitrobenzeno-2-oxa-1,3-diazole actin as a probe for actin polymerization. *J. Biol. Chem.* **256**, 99–105.
- Espreafico, E.M., Cheney, R.E., Matteoli, M., Nascimento, A.A., De Camilli, P.V., Larson, R.E., and Mooseker, M.S. (1992). Primary structure and cellular localization of chicken brain myosin-V (p190), an unconventional myosin with calmodulin light chains. *J. Cell Biol.* **119**, 1541–1557.
- Fisher, G.W., Conrad, P.A., DeBiasio, R.L., and Taylor, D.L. (1988). Centripetal transport of cytoplasm, actin, and the cell surface in lamellipodia of fibroblasts. *Cell Motil. Cytoskel.* **11**, 235–247.
- Forscher, P., and Smith, S.J. (1988). Actions of cytochalasins on the organization of actin filaments and microtubules in a neuronal growth cone. *J. Cell Biol.* **107**, 1505–1516.
- Forscher, P., and Smith, S.J. (1990). Cytoplasmic actin filaments move particles on the surface of a neuronal growth cone. In *Optical Microscopy for Biology*. (New York: Wiley-Liss), pp. 459–471.
- Forscher, P., Lin, C.-H., and Thompson, C. (1992). Novel form of growth cone motility involving site-directed actin filament assembly. *Nature* **357**, 515–518.
- Fryer, M.W., Neering, L.R., and Stephenson, D.G. (1988). Effects of 2,3-butanedione monoxime on the contractile activation properties of fast- and slow-twitch rat muscle fibers. *J. Physiol. (Lond.)* **407**, 53–75.
- Grazi, E., Ferri, A., Lanzara, V., Magri, E., Zaccarini, M. (1980). G-actin modified by plasma membrane interaction polymerizes only in the presence of filamentous myosin. *FEBS Lett.* **112**, 67–69.
- Gwathmey, G.K., Hajjar, R.J., and Solaro, J.R. (1992). Contractile deactivation and the uncoupling of crossbridge: effects of 2,3-butanedione monoxime. *Circ. Res.* **69**, 1280–1292.
- Heath, J.P., and Holifield, B.F. (1991). Cell locomotion: new research tests old idea on membrane and cytoskeletal flow. *Cell Motil. Cytoskel.* **18**, 245–257.
- Herrmann, C., Wray, J., Travers, F., and Barman, T. (1992). Effect of 2,3-butanedione monoxime on myosin and myofibrillar ATPase: an example of an uncompetitive inhibitor. *Biochemistry* **31**, 12227–12232.
- Higuchi, H., and Takemori, S. (1989). Butanedione monoxime suppresses contraction and ATPase activity of rabbit skeletal muscle. *J. Biochem.* **105**, 638–643.
- Horiuti, K., Higuchi, H., Umazume, Y., Konoshi, M., Okazaki, O., and Kurihara, S. (1988). Mechanisms of action of 2,3-butanedione 2-monoxime on contraction of frog skeletal muscle fibers. *J. Muscle Res. Cell Motil.* **9**, 156–164.
- Kennedy, T.E., and Tessier-Lavigne, M. (1995). Guidance and induction of branch formation in developing axons by target-derived diffusible factors. *Curr. Opin. Neurobiol.* **5**, 83–90.
- Kielley, W.W., and Harrington, W.F. (1959). A model for myosin molecule. *Biochim. Biophys. Acta* **41**, 401–421.
- Lee, J., Ishihara, A., Theriot, J.A., and Jacobson, K. (1993). Principles of locomotion for simple-shaped cells. *Nature* **362**, 167–171.
- Lee, J., Leonard, M., Oliver, T., Ishihara, A., and Jacobson, K. (1994). Traction forces generated by locomoting keratocytes. *J. Cell Biol.* **127**, 1957–1964.
- Lewis, A.K., and Bridgman, P.C. (1992). Nerve growth cone lamellipodia contain two populations of actin filaments that differ in organization and polarity. *J. Cell Biol.* **119**, 1219–1243.
- Lin, C.-H., and Forscher, P. (1993). Cytoskeletal remodeling during growth cone-target interactions. *J. Cell Biol.* **121**, 1369–1383.
- Lin, C.-H., and Forscher, P. (1995). Growth cone advance is inversely proportional to retrograde F-actin flow. *Neuron* **14**, 763–771.
- Lin, C.-H., Thompson, C.A., and Forscher, P. (1994). Cytoskeletal reorganization underlying growth cone motility. *Curr. Opin. Neurobiol.* **4**, 640–647.
- Margossian, S.S., and Lowey, S. (1982). Preparation of myosin and its subfragments from rabbit skeletal muscle. *Meth. Enzymol.* **85**, 55–71.
- McKillop, K.F., Fortsne, N.S., Ranatunga, K.W., and Geeves, M.A. (1994). The influence of 2,3-butanedione-2-monoxime on the interactions between actin and myosin in solution and skinned muscle fibers. *J. Muscle Res. Cell Motil.* **15**, 309–318.
- Meeusen, R.L., and Cande, W.Z. (1979). N-Ethylmaleimide modified heavy meromyosin: a probe for actomyosin interactions. *J. Cell Biol.* **82**, 57–65.
- Miller, L., Phillips, M., and Reisler, E. (1988). Polymerization of G-actin by myosin subfragment 1. *J. Biol. Chem.* **4**, 1996–2002.
- Miller, M., Bower, E., Levitt, P., Li, D., and Chantler, P.D. (1992). Myosin II distribution in neurons is consistent with a role in growth cone motility but not synaptic vesicle mobilization. *Neuron* **8**, 25–44.
- Mitchison, T., and Kirschner, M. (1988). Cytoskeletal dynamics and nerve growth. *Neuron* **1**, 761–772.
- Mooseker, M.S., and Cheney, R.E. (1995). Unconventional Myosins. *Annu. Rev. Cell Biol.* **11**, 633–675.

- Pollard, T.D. (1986). Rate constants for the reactions of ATP- and ADP-actin with the ends of actin filaments. *J. Cell Biol.* 103, 2747–2754.
- Pollard, T.D., and Cooper, J.A. (1986). Actin and actin-binding proteins: a critical evaluation of mechanisms and functions. *Annu. Rev. Biochem.* 55, 987–1035.
- Rochlin, M.W., Itoh, K.I., Adelstein, R.S., and Bridgman, P.C. (1995). Localization of myosin II A and B isoforms in cultured neurons. *J. Cell Sci.* 108, 3661–3670.
- Ruppert, C., Kroschewski, R., and Bahler, M. (1993). Identification, characterization and cloning of myr 1, a mammalian myosin-I. *J. Cell Biol.* 120, 1393–1403.
- Schramm, M., Klieber, H.G., and Daut, J. (1994). The energy expenditure of actomyosin ATPase, calcium-ATPase and sodium-potassium-ATPase in guinea pig cardiac ventricular muscle. *J. Physiol.* 481, 647–662.
- Smith, S.J. (1988). Neuronal cytomotility: the actin-based motility of growth cones. *Science* 242, 708–715.
- Spudich, J.A., and Watt, S. (1971). The regulation of rabbit skeletal muscle contraction. I. Biochemical studies of the interaction of the tropomyosin-troponin complex with actin and the proteolytic fragments of myosin. *J. Biol. Chem.* 246, 4866–4871.
- Steele, D.S., and Smith, G.L. (1993). Effects of 2,3-butanedione monoxime on sarcoplasmic reticulum of saponin-treated rat cardiac muscle. *Am. J. Physiol.* 265, H1493–1500.
- Steinen, G.J.M., Zaremba, R., and Elzinga, G. (1995). ATP utilization for calcium uptake and force production in skinned muscle fibers of *Xenopus laevis*. *J. Physiol.* 482, 109–122.
- Svoboda, K., and Block, S.M. (1994). Biological applications of optical forces. *Annu. Rev. Biophys. Biomol. Struct.* 23, 247–285.
- Tanaka, E., and Sabry, J. (1995). Making the connection: cytoskeletal rearrangements during growth cone guidance. *Cell* 83, 171–176.
- Tessier-Lavigne, M. (1992). Axon guidance by molecular gradients. *Curr. Opin. Neurobiol.* 2, 60–65.
- Theriot, J.A., and Mitchison, T.J. (1991). Actin microfilament dynamics in locomoting cells. *Nature* 352, 126–131.
- Theriot, J.A., and Mitchison, T.J. (1992a). The nucleation-release model of actin filament dynamics in cell motility. *Tr. Cell Biol.* 2, 219–222.
- Theriot, J.A., Mitchison, T.J., Tilney, L.G., and Portnoy, D.A. (1992b). The rate of actin-based motility of intracellular *Listeria monocytogenes* equals the rate of actin polymerization. *Nature* 357, 257–260.
- Tung, L., Sperelakis, N., Ten Erick, R.E., and Solaro, R.J. (1985). Effects of diacetyl monoxime on cardiac excitation-contraction coupling. *J. Pharm. Exp. Ther.* 232, 688–695.
- Wang, Y.L. (1985). Exchange of actin subunits at the leading edge of living fibroblasts: possible role of treadmilling. *J. Cell Biol.* 101, 597–602.
- West, J.M., and Stephenson, D.G. (1989). Contractile activation and the effects of 2,3-butanedione monoxime (BDM) in skinned cardiac preparation from normal and dystrophic mice (129/ReJ). *Pflügers Arch.* 413, 546–552.
- Yamada, K.M., and Wessells, N.K. (1973). Cytochalasin B: effects on membrane ruffling, growth cone and microspike activity, and microfilament structure not due to altered glucose transport. *Dev. Biol.* 37, 413–420.
- Zhao, Y., and Kawai, M. (1994). BDM affects nucleotide binding and force generation steps of the crossbridge cycle in rabbit psoas muscle fibers. *Am. J. Physiol.* 266, C437–447.